Topology-Driven Performance Analysis of Power Grids

Çetinay, Hale; Koç, Yakup; Kuipers, Fernando A.; Van Mieghem, Piet

Important note
To cite this publication, please use the final published version (if applicable).
Please check the document version above.

Chapter 2
Topology-Driven Performance Analysis of Power Grids

Hale Çetinay, Yakup Koç, Fernando A. Kuipers and Piet Van Mieghem

Abstract   Direct connections between nodes usually result in efficient transmission in networks. Such electric power transmission is governed by physical laws, and an assessment purely based on direct connections between nodes and shortest paths may not capture the operation of power grids. Motivated by these facts, in this chapter, we investigate the relation between the electric power transmission in a power grid and its underlying topology. Initially, we focus on synthetic power grids whose underlying topology can be structured as either a path or a complete graph. We analytically compute the impact of electric power transmission on link flows under the normal operation and under a link failure contingency using the linearised DC power flow equations. Subsequently, in various other graph types, we provide empirical results on the link flow, the voltage magnitude and the total active power loss in power grids using the nonlinear AC power flow equations. Our results show that in a path graph, as an assessment based on shortest paths holds, however, the electric power transmission can lead to substantial amount of link flows, active power loss and voltage drops, especially in large path graphs. On the other hand, adding few links to a path graph could significantly improve those performance indicators of power grids, but at a cost: the resulting meshed topology decreases the control over power grids

H. Çetinay (✉) · F. A. Kuipers · P. Van Mieghem
Faculty of Electrical Engineering, Mathematics and Computer Science, P.O Box 5031,
2600 GA Delft, The Netherlands
e-mail: H.Cetinay-Iyicil@tudelft.nl

F. A. Kuipers
e-mail: F.A.Kuipers@tudelft.nl

P. Van Mieghem
e-mail: P.F.A.VanMieghem@tudelft.nl

Y. Koç
Risk Management Group, Asset Management, Stedin B.V., 2628 CD Delft, The Netherlands
e-mail: yakupkoc@gmail.com

Y. Koç
Systems Engineering, Technology Policy and Management, Delft University of Technology,
2628 CD Delft, The Netherlands

as a direct assessment between the shortest paths and the electric power transformation is lost. Additionally, a meshed topology with loops increases the redundancy in the design to ensure a safe operation under a link failure contingency.

2.1 Introduction

Many researchers analyse power grids from a graph topological point of view [1, 2]. Various topology metrics (such as nodal degree, clustering coefficient) have been proposed to assess the vulnerability or to locate the critical components of power grids [3–5]. Those purely topological approaches, however, may fail to fully capture the physical and operational specific features of power grids whose operation are governed by physical laws.

In this chapter, we take an extended graph theoretical approach [6–8] by modelling the electrical properties such as flow allocation according to Kirchhoff's laws and the impedance values of transmission lines in power grids. We investigate the impact of network topology on the key performance indicators of power grids, which we take as the node voltage, the link flow, the total power loss and the served electric demand.

Initially, we focus on the operation by considering two extreme graphs. In synthetic power grids whose underlying topology is either a path or a complete (full-mesh) graph, we analytically derive the steady-state operating conditions under normal operation and under a random link failure (removal) contingency using the linearised DC power flow equations. Subsequently, in various other graphs, we empirically investigate the relation between the topology and the key performance indicators using the nonlinear AC power flow equations [9].

The remainder of this chapter is organized as follows. Section 2.2 investigates the electric power transmission in path and complete graphs under normal operation. In Sect. 2.3, we focus on single link failure contingencies in those graphs, and derive the impact of a random link failure on the steady-state link flows. Section 2.4 presents our empirical results on the key performance indicators in various graphs both under normal operation and single link failure contingencies. Section 2.5 concludes the chapter.

2.2 DC Power Flow Analysis in Path and Complete Graphs

A connected simple graph (i.e., a graph with no parallel duplicate links or self-loops) lies between a complete graph and a tree graph. In a complete graph, every pair of distinct nodes is connected by a link. On the other hand, a tree has no cycles; consequently, any two nodes are connected by exactly one path.

The direct connections between nodes usually result in an efficient transmission in a network. The distances between the nodes in a complete graph are shortest com-

pared to the other graphs, in which multiple hops are needed to reach the destination. In power grids, different than the typical transmissions based on the shortest paths, the electric power transmission is governed by physical laws. Therefore, an assessment based on purely the direct connections between nodes may not be enough to draw conclusions. In this section, we investigate the electric power transmission in those extreme graph types.

We model power grids with N buses (nodes), and L lines (links) by a weighted graph $G(N, L)$. We use $\mathcal{N}$ to denote the set of N nodes and $\mathcal{L}$ to denote the set of L links with equal weights, b. Every link $l_{ik} \in \mathcal{L}$ is associated with a maximum flow capacity C_{ik} that represents the maximum power flow that can be afforded by the corresponding line, and a rest flow capacity $\alpha_{ik} = C_{ik} - |f_{ik}|$ where $|f_{ik}|$ is the flow through the link l_{ik} under normal operation. We assume a single upstream *supply* node, and treat the remaining $N - 1$ downstream nodes as *demand* nodes. Without loss of generality, we label the supply node as node 1, and take the total electric power demand of the network as $(N - 1)p$ where $p \geq 0$ is a constant. Throughout Sects. 2.2 and 2.3, we adopt the slack-bus independent solution to the DC power flow equations [10], which could approximate the steady-state operation under the DC power flow assumptions [11].

2.2.1 Electric Power Transmission in a Path Graph

We investigate the electric power transmission from the supply node 1 to the single demand node N in a path graph (whose nodes are labeled consecutively). The magnitude $|f_{ik}^{1 \to N}|$ of the flow through a link l_{ik} between node i and node $k = i + 1$ is found as (see Sect. 2.6.1)

$$
\begin{aligned}
|f_{ik}^{1 \to N}| &= b|(\theta_i - \theta_k)| \\
&= p(N - 1) \quad \forall l_{ik} \in \mathcal{L},
\end{aligned} \tag{2.1}
$$

where b is the reciprocal of the line reactance and θ_i is the phase angle of the voltage at node i.

Equation (2.1) shows that the resulting link flows due to the electric power transmission are all the same, and their values increase with the increasing graph size N and unit power demand p. This linear correlation between the size and the magnitudes of link flows could lead to substantial flows and result in congestion problems, especially in large graphs.

On the other hand, in a path graph, the electric power is transferred through a single path between the supply and the demand node. Consequently, an assessment based on shortest paths holds, which can ease the supervision of the network operator.

2.2.2   Electric Power Transmission in a Complete Graph

Similar to Sect. 2.2.1, we investigate the electric power transmission from the supply node 1 to a single (randomly chosen) demand node m in a complete graph. The magnitude $|f_{ik}^{1\to m}|$ of the resulting flow through a link l_{ik} is found as (see Sect. 2.6.2)

$$|f_{ik}^{1\to m}| = \begin{cases} \frac{2(N-1)p}{N} & \text{if } l_{ik} = l_{1m}, \\ \frac{(N-1)p}{N} & \text{if } l_{ik} \in \big\{\big(\mathcal{B}(1) \cup \mathcal{B}(m)\big) \setminus l_{1m}\big\}, \\ 0 & \text{otherwise,} \end{cases} \tag{2.2}$$

where $\mathcal{B}(i)$ denotes the direct neighbors of node i.

Equation (2.2) indicates that three different magnitudes of link flow exist during the electric power transmission: (a) The flow through the link between the supply and the demand node is maximum, whereas (b) the flows through the links to the other neighbors of those nodes are half of that maximum flow, and (c) the remaining links that are not direct neighbors of either the supply or the demand node have zero flows.

Comparing the magnitudes of link flow in a path graph in Eq. (2.1) and a complete graph in Eq. (2.2) shows that the maximum link flow due to the electric power transmission from the supply node to a demand node is dramatically lower in a complete graph. However, the distribution of the flows through links in a complete graph is not homogeneous, thus the relation between the total decrease in the magnitudes of link flow and the total number of links added to a path graph is not linear.

2.3   DC Power Flow Analysis in Path and Complete Graphs After a Random Link Failure

Single line failures are common in power grids. Therefore, as well as under the normal operation, the operation after a link failure (removal) is important to assess the reliability of power grids [12]. In this section, we theoretically investigate the effect of a random link failure on link flows in path and complete graphs using the linearised DC power flow equations. In addition, to quantify the effect of link failure contingencies in a graph, we calculate the *theoretical robustness function* of those graphs, which we define as the expected fraction of served demands after a random link failure.

2.3.1   Random Link Failure in a Path Graph

First, we focus on the effect of a single link failure in path graphs. Just before the link failure takes place, we assume that all demand nodes have a unit electric power

demand of p, which we refer to as the *symmetrical distribution* of demands. In other words, the supply node transfers a unit electric power of p to every other demand node, resulting in the magnitude $|f_{ik}|$ of the flow through link l_{ik} between node i and node $k = i + 1$ before the failure

$$|f_{ik}| = p(N - i). \tag{2.3}$$

As the graph under investigation is a path graph with no cycles, the removal of any link l_{ik} between node i and node $k = i + 1$ partitions the graph (see Sect. 2.6.3), and this partition removes in total $p \times (N - i)$ demand from the graph according to Eq. (2.3). Therefore, the closer the link failure is to the supply node 1, the worse is the effect on the served demands.

The continuity of the operation of the network depends on the location of the failed link. If the failed link is adjacent to the supply node, then the supply node is isolated from the demand nodes and the network faces a complete blackout. If the failure probabilities of the links are the same in a path graph, the probability p_b that a random link failure leads to a complete blackout is $p_b = \frac{1}{L} = \frac{1}{N-1}$.

The failure and removal of any other link partitions the network and the remaining network can continue functioning, though with decreased demands. As the total demand of the network decreases after the link removal, the flows through the remaining links decrease, and thus, there is no possibility for further cascading failures [13] due to the insufficient rest flow capacity of the remaining links. Consequently, the expected fraction $E[F_s]$ of served demands after a random link failure is

$$E[F_s] = \frac{1}{N - 1} \times \frac{(0 + 1 + \cdots + N - 2)}{N - 1} = \frac{N - 2}{2(N - 1)}.$$

2.3.2 Random Link Failure in a Complete Graph

Next, we investigate a random link failure in a complete graph. After the removal of a link, the flows are redistributed following Kirchhoff's laws and the flows through the remaining links may change. Due to the meshed topology of the graph, this redistribution can lead to an increase or a decrease in flow through a particular link [10].

Before a link failure happens, under symmetrical distribution of demands, i.e., when the supply node transfers a unit demand of p to every other demand node, the magnitude $|f_{ik}|$ of the flow through a link l_{ik} in a complete graph is

$$|f_{ik}| = \begin{cases} p & \text{if } l_{ik} \in \mathcal{B}(1), \\ 0 & \text{otherwise.} \end{cases} \tag{2.4}$$

Following Eq. (2.4), two different magnitudes of link flows exist in a complete graph under the symmetrical distribution of demands. As a result, a single link failure and removal can result in two cases:

Failure of a Link with Zero Flow

When a link l_{ik} is removed from the graph, the flow $|f_{ik}|$ through the link before failure needs to be redistributed over the alternative paths between nodes i and k. Since a *redundant* link l_{ik} does not transport any flow, its removal does not cause a power redistribution.

Failure of a Link with Maximum Flow

When a *used* link l_{ik} is removed from the graph, the flow $|f_{ik}| = p$ through the link before failure is redistributed over alternative paths between nodes i and k. As a result, the initial link l_{ik} failure may trigger further failures in the network if the increase $|\Delta f_{ab}| = \frac{p}{N-2}$ in the flow through a remaining link l_{ab} exceeds its rest flow capacity α_{ab} (see Sect. 2.6.4),

$$|\Delta f_{ab}| = \frac{p}{N - 2} \geq \alpha_{ab}. \tag{2.5}$$

When the rest flow capacity α_{ab} is smaller than the required value in Eq. (2.5), consecutive failures occur. After the initial failure of the used link l_{ik}, the flows through all remaining used links exceed their maximum flow capacity, and fail in the next stage of the failure. This isolates the supply node. Consequently, the remaining network cannot match any demands, and it could face a complete blackout.

When the size N of the graph is 2, i.e., when there is only one link, the failure of that link destroys the graph by separating the supply node from the demand node regardless of the rest flow capacity α_{ab} of the link. For larger graphs, Eq. (2.5) shows the required rest flow capacity α_{ab} of links is maximum when the size of the graph is $N = 3$, whereas it decreases as N increases. This means the effect of a link removal on the flows through the remaining links reduces with the size N of the graph.

Finally, we calculate the *theoretical robustness function* of a complete graph, which is the expected fraction $E[F_s]$ of served demands after a random link removal from the underlying graph. Figure 2.1 presents the theoretical robustness function of a complete graph under the symmetrical distribution of demands. If the rest flow capacity of the links is larger than the required value in Eq. (2.5), the remaining links can tolerate the redistributed flows after a random link removal. The network can continue to serve the same amount of total demand after any single link failure. Therefore, in region II in Fig. 2.1, the fraction of served demands stays the same. On the other hand, when the rest flow capacity of the links is smaller than the required value in Eq. (2.5) in region I, the network continues its operation only if the failed link is a *redundant* link with zero flow. Otherwise, when a *used* link with flow p fails, the network faces complete blackout and cannot serve any demand. Therefore, the expected $E[F_s]$ fraction of served demands after a random link failure in region I is calculated as

Fig. 2.1 The expected $E[F_s]$ fraction of served demands versus the rest flow capacity of the links after a random link failure in a complete graph under symmetrical distribution of demands. The figure is computed for $N = 5$
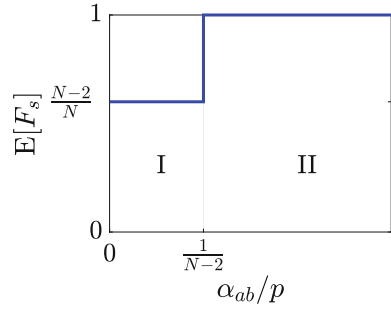
$$E[F_s] = 1 \times p_r + 0 \times p_u = \frac{N-2}{N} = 1 - \frac{2}{N},$$

where $p_r = \frac{N-2}{N}$ represents the probability that the failed link is a redundant link with zero flow and $p_u = \frac{2}{N}$ represents the probability that the failed link is a used link with flow p (see Eqs. (2.16) and (2.17)).

Comparing the effect of single link failures in a path and a complete graph shows that a path (or a tree) cannot provide a back-up path after a link removal, and the total served demand in the network definitely decreases. In addition, as the demands in the network decrease, there is no possibility of cascading failures in a tree graph with no loops. On the other hand, a meshed topology can provide back-up paths during random link removals. Yet, the correct setting of design parameters, i.e., the rest flow capacities of the links, is extremely important. If the rest flow capacity α_{ab} of the links is smaller than in Eq. (2.5) and a used link fails, then the remaining links in a complete graph cannot tolerate the redistributed flows. Consequently, a random link removal in a complete graph could lead to more link and demand losses than a link failure in a simple path graph.

2.4 Impact of Topology on Key Performance Indicators of Power Grids

In Sects. 2.2 and 2.3, we focus on the theoretical analyses of electric power transmission in path and complete graphs. In this section, we focus on many other graphs and empirically investigate the key performance indicators of power grids under normal operation as well as under single link failure contingencies. In our analyses, we use the AC power flow solver in Matlab [9] to calculate the steady-state operating conditions under the symmetrical distribution of demands. In addition to the line reactance x and the active power p values, we take into account the line resistance r and the reactive power q values for a more practical model of power grids.

2.4.1 Key Performance Indicators Under Normal Operation

For the safe and efficient operation of power grids, lower magnitudes of link flow and total power loss, and higher values of node voltage (close to 1 per unit) are desired.[1] In a power grid whose topology are modelled by the specific graph G, we define the satisfaction degree of performance indicators of link flow $\zeta(G)$, node voltage $v(G)$ and power loss $\eta(G)$ as

$$
\zeta(G) = \begin{cases} 1 & \text{if } \max_{l_{ik}\in\mathcal{L}(G)} \left(|f_{ik}|\right) < p, \\ \frac{\tau_f - \max_{l_{ik}\in\mathcal{L}(G)}\left(|f_{ik}|\right)}{\tau_f - p} & \text{if } p \leq \max_{l_{ik}\in\mathcal{L}(G)} \left(|f_{ik}|\right) \leq \tau_f, \\ 0 & \text{if } \max_{l_{ik}\in\mathcal{L}(G)} \left(|f_{ik}|\right) > \tau_f, \end{cases} \tag{2.6}
$$

$$
v(G) = \begin{cases} 0 & \text{if } \min_{i\in\mathcal{N}(G)} \left(v_i\right) < \tau_v, \\ \frac{\min_{i\in\mathcal{N}(G)}\left(v_i\right) - \tau_v}{1 - \tau_v} & \text{if } \tau_v \leq \min_{i\in\mathcal{N}(G)} \left(v_i\right) \leq 1, \\ 1 & \text{if } \min_{i\in\mathcal{N}(G)} \left(v_i\right) > 1, \end{cases} \tag{2.7}
$$

$$
\eta(G) = \begin{cases} 1 & \text{if } \tau_\sigma < 0, \\ \frac{\tau_\sigma - \sigma(G)}{\tau_\sigma} \leq \tau_f, & \text{if } 0 \leq \sigma(G) \leq \tau_\sigma, \\ 0 & \text{if } \sigma(G) > \tau_\sigma, \end{cases} \tag{2.8}
$$

where $|f_{ik}|$ is the magnitude of the flow through link l_{ik}, v_i is the magnitude of voltage at node i, $\sigma(G)$ is the total active power loss, and $\mathcal{L}(G)$ and $\mathcal{N}(G)$ denote the set of links and nodes of graph G, respectively. The performances in Eqs. (2.6)–(2.8) are evaluated on a scale from 0 to 1 (see Fig. 2.2): The highest performance of 1 corresponds to *ideal power grids* in which the maximum link flow is equal to the unit power demand p, the minimum voltage is equal to 1 per unit, i.e., no voltage drop, and the total power loss is 0, i.e., a lossless power grid. Conversely, the lowest performance of 0 corresponds to the maximum link flow τ_f, the minimum node voltage τ_v and the total power loss τ_σ. The requirements of τ_f, τ_v and τ_σ are usually determined by the specific grid codes of the operators.

Figure 2.3 shows the variations of the key performance indicators under the symmetrical demand distribution throughout the topological transformation of the path graph with 5 nodes and 4 links.[2] Figure 2.3 depicts that the performance indicator of link flow is lowest in the path, and highest in the complete graph. We observe that the cycle graph *dramatically increases the performance indicator of link flow* by decreasing the maximum link flow compared to the path graph. Similar to the

---

[1]As we focus on the impact of electric power transmission from a supply node to demand nodes, only voltage drops in the network are considered.

[2]We compute all possible ways to evaluate the transformation from the path to the complete graph, which is only possible for small graphs.
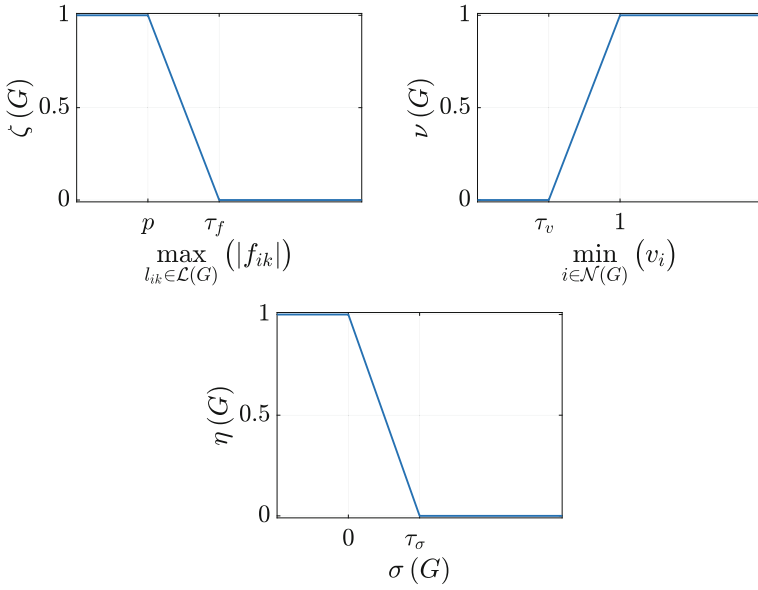
Fig. 2.2 The functions of the performance indicators of link flow $\zeta(G)$, node voltage $\nu(G)$ and power loss $\eta(G)$
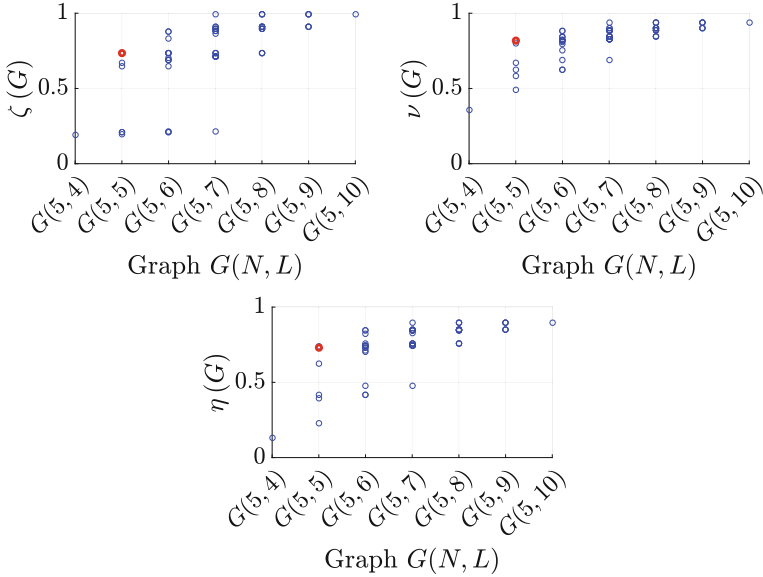

Fig. 2.3 The variations of the key performance indicators throughout the topological transformation of the path graph $G(5, 4)$ with 5 nodes and 4 links. The transformation towards the complete graph $G(5, 10)$ requires the addition of $\frac{N(N-1)}{2} - (N-1) = 6$ links, which can be performed in $2^6 - 1 = 63$ different ways. The bold red data point corresponds to the cycle graph. The performance indicators are evaluated for $r = 0.1$, $x = 0.1$, $p = 0.05$, $q = 0.01$, $\tau_f = 5p$, $\tau_v = 0.9$ and $\tau_\sigma = 0.2p$
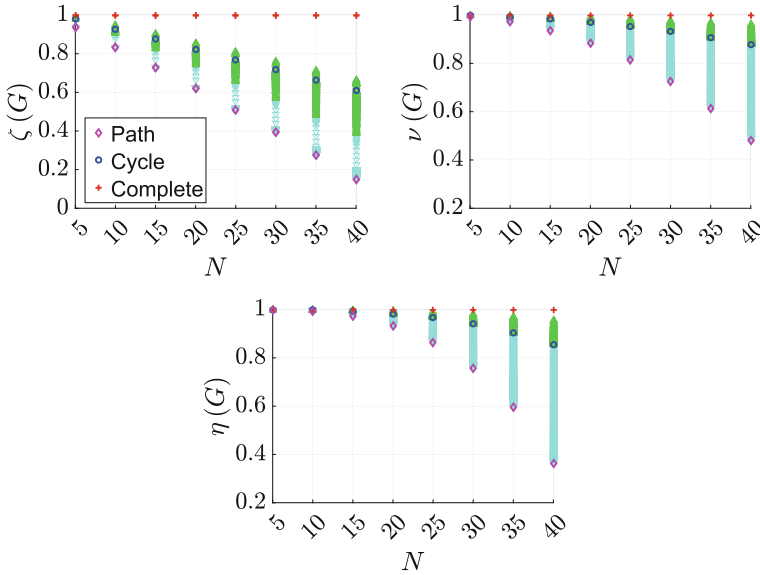
Fig. 2.4 The variations of the key performance indicators in graphs with different sizes N. The blue lower triangle ($\triangledown$), and green upper triangle ($\triangle$) data points correspond to the graphs that are constructed by adding one link to the path graph, and adding one link to the cycle graph, respectively. The performance indicators are evaluated for $r = 0.02, x = 0.02, p = 0.005, q = 0.001, \tau_f = 50p$, $\tau_v = 0.8$ and $\tau_\sigma = 4p$

link flows, the minimum voltage is lowest and the total power loss is highest in the path graph. The complete graph, on the other hand, represents the operation at the minimum voltage drop and total power losses, thus corresponding to the highest values of key performance indicators.

Figure 2.3 indicates that a meshed topology can improve the key performance indicators compared to the path graph. We showed in Eq. (2.2) that the flow distribution in a complete graph due to an electric power transmission is not homogeneous, which could explain the nonlinear relation between the total number of added links to the path graph and the total increase in the key performance indicators in Fig. 2.3. In particular, the cycle graph and the *augmented cycles*, i.e., the graphs constructed from the cycle graph by adding links, are observed to affect the key performance indicators dramatically.

In Fig. 2.4, we present the variations of key performance indicators in the graphs with different sizes N. In the complete graphs, the maximum link flows are nearly the same for all sizes N, which is in agreement with the theoretical calculations in Eq. (2.4). In the other graphs, the maximum link flow increases with increasing size N, decreasing the performance indicator of link flow.

From Fig. 2.4, we observe that the minimum values of node voltages are nearly the same in the complete graphs, whereas they decrease dramatically in the path graphs with increasing size N. On the other hand, the cycle topology increases the node

voltages, thus also the performance indicator of node voltage, rapidly compared to the path graph.

Similar observations hold for the performance indicator of power loss. In large path graphs, the total active power loss of the network is high, which decreases the performance indicator of power loss. On the other hand, a complete graph nearly zeroes the power loss and the cycle topology significantly decreases the total loss compared to a path graph.

Similar to Figs. 2.3 and 2.4 illustrates that a meshed topology can improve the key performance indicators compared to a path graph. We conclude that the core contributions to the key performance indicators arise from the first few links added to a path graph. In particular, for larger graphs, a cycle topology can dramatically increase the voltage magnitude and decrease total active power loss of the network compared to the path graph. Consequently, adding a limited number of links to the tree topology can still achieve higher levels of performance during the electric power transmission between a supply and demand nodes.

2.4.2   Key Performance Indicators Under a Single Link Failure Contingency

In this section, we investigate the effect of a single link failure in different graphs. Initially, we focus on the effect of a link failure on the served demands of the network. Figure 2.5 illustrates the expected $E[F_s]$ fraction of served demands after a random link failure throughout the topological transformation of a path graph $G(5, 4)$ with 5 nodes and 4 links. In Sect. 2.3, we show that any link removal from a path graph partitions the graph. Figure 2.5 also depicts that only a cycle or augmented cycles can provide a back-up after any random link failure. The other graphs may partition after a random link failure and can continue their operation only with a decreased
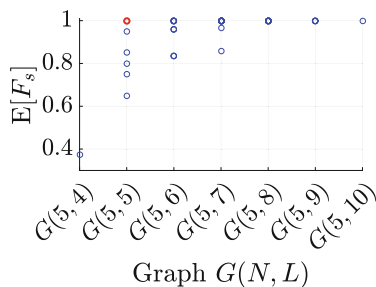

Fig. 2.5 The expected $E[F_s]$ fraction of served demands after a random link failure throughout the topological transformation of a path graph with 5 nodes. The bold red data point corresponds to the cycle graph. The remaining links are assumed to have enough rest flow capacity to handle the redistributed flows due to a random link failure
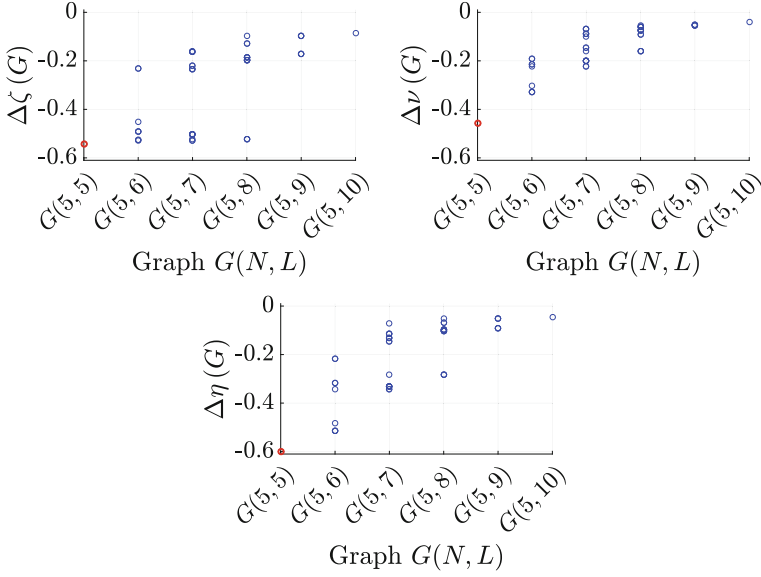
Fig. 2.6 The variations of the changes Δ in the key performance indicators after a link failure throughout the topological transformation of a path graph with 5 nodes. The bold red data point corresponds to the cycle graph. The performance indicators are evaluated for $r = 0.1$, $x = 0.1$, $p = 0.05$, $q = 0.01$, $\tau_f = 5p$, $\tau_v = 0.9$ and $\tau_\sigma = 0.2p$

total demand, which usually improves the key performance indicators. Therefore, in this subsection, we only focus on the graphs that can provide a back-up after any random link failure.

To investigate and compare the effect of single link failures in each graph, we removed one link at a time from the graph, and calculated the changes in the performance indicators. We repeated this link failure contingency simulation for each link, and compared all changes in the link flow, the node voltage and the active power loss in the network. Figure 2.6 illustrates the maximum resulting changes in these key performance indicators after a link removal throughout the topological transformation of a path graph $G(5, 4)$ with 5 nodes and 4 links. The performance indicator of link flow can significantly decrease after a link failure in a cycle graph. For the complete graph, on the other hand, we observe that the effect of a link failure on the indicator of link flow is very small. Similar to the changes in the indicator of link flow, the decreases in the performance indicators of node voltage and power loss are highest in the cycle graph after a single link failure.

Finally, in Fig. 2.7, we present the variations of key performance indicators after a link failure in graphs with different sizes N. Similar to the theoretical calculation in Eq. (2.5), the effect of a link failure on the remaining link flows slightly decreases with the increasing size N in the complete graphs. On the other hand, in cycle graphs, the change in the magnitude of the flow through a remaining link can significantly increase with the increasing size N, which decreases the related performance indi-
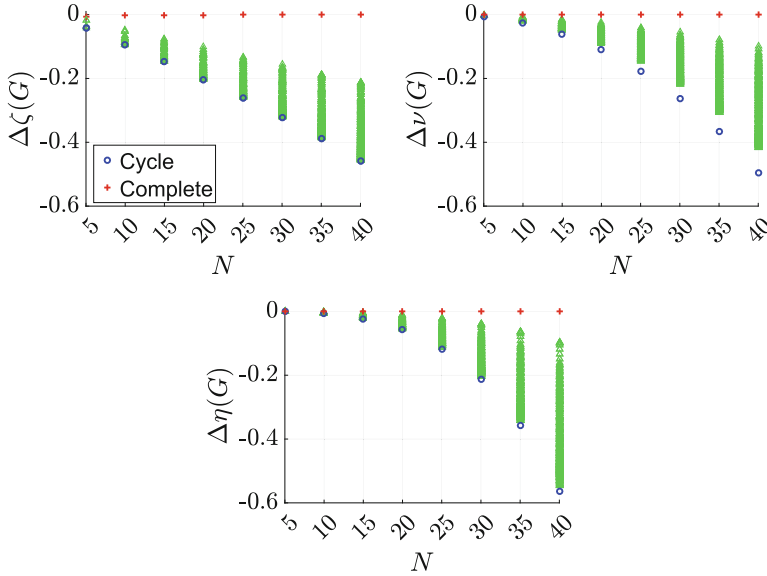
Fig. 2.7 The variations of the changes Δ in the key performance indicators after a link failure in graphs with different sizes N. The green upper triangle ($\triangle$) data points correspond to the graphs that are constructed by adding one link to the cycle graph. The performance indicators are evaluated for $r = 0.02$, $x = 0.02$, $p = 0.005$, $q = 0.001$, $\tau_f = 50p$, $\tau_v = 0.8$ and $\tau_\sigma = 4p$

cator. In the *worst* case, when one of the links adjacent to the supply node fails in a cycle graph, it operates as a path graph with the same size N after the link failure. Therefore, the performance indicator of link flow in a cycle graph under a single link failure contingency becomes the performance indicator of link flow in a path graph under normal operation.

Similar to the changes in the performance indicator of link flow after a link failure, the indicators of node voltage and power loss slightly decrease in a complete graph with increasing size N. In the other graphs, however, the decrease in the key performance indicators could be drastic. Although under the normal operation, the cycle and the augmented cycles can provide higher values of the performance indicators; after a link failure, large drops on the key performance indicators in those graphs are expected.

2.5 Conclusion

In this chapter, we investigated the impact of topology on the electric power transmission and the performance of power grids. By utilizing a graph theoretical approach, we first focused on two extreme graphs, complete and path graphs, and analysed the electric power transmission under normal operation and under single link failure

contingencies. We showed that in complete graphs, due to the redistributed flows, the survival of power grids from a random link failure depends on the rest flow capacity of the remaining links. Consequently, when the rest flow capacities are insufficient to handle the redistributed flows, a single link failure could result in more link and demand loss in a complete graph than in a path graph.

Subsequently, we empirically investigated the effect of the electric power transmission on the link flow, the node voltage and the active power loss in power grids in various other graphs. Our results show that adding few links to a path graph can significantly improve these key performance indicators of power grids compared to a path graph. However, at the same time, the performance indicators could also remarkably decrease after a link failure. Consequently, throughout a topological transformation towards a meshed topology with loops, redundancies in the design parameters of power grids are needed to ensure safety under normal operation and as well as under single link failure contingencies.

Appendix

2.6 DC Power Flow Equations in Extreme Graph Types

We model power grids with N buses (nodes), and L transmission lines (links) by a weighted graph $G(N, L)$. The $N \times N$ weighted adjacency matrix $\mathbf{W}$ specifies the interconnection pattern of the graph $G(N, L)$: w_{ik} is non-zero only if the nodes i and k are connected by a link; otherwise $w_{ik} = 0$. In the slack-bus independent solution of the DC power flow equations [10], the relation between the phase angles $\Theta = [\theta_1 \ldots \theta_N]^T$ of node voltages, and the power input $\mathbf{P} = [p_1 \ldots p_N]^T$ is given as [10]

$$\Theta = \mathbf{Q}^+ \mathbf{P}, \tag{2.9}$$

where $\mathbf{Q}^+$ is the pseudo inverse of the Laplacian $\mathbf{Q}$ of the weighted graph $G(N, L)$.

2.6.1 Operating Conditions in a Path Graph

For a path graph, whose nodes are numbered consecutively and links have equal link weights $b > 0$, the structure of weighted Laplacian $\mathbf{Q}$ can be written as

$$\mathbf{Q} = \begin{bmatrix} b & -b & 0 & \ldots & 0 & 0 \\ -b & 2b & -b & 0 & \ldots & 0 \\ 0 & \ddots & \ddots & \ddots & & \vdots \\ \vdots & & \ddots & \ddots & \ddots & 0 \\ 0 & \ldots & 0 & -b & 2b & -b \\ 0 & 0 & \ldots & 0 & -b & b \end{bmatrix}.$$

In order to find $\mathbf{Q}^+$ in Eq. (2.9), we use the definition [14] of the pseudo-inverse of Laplacian $\mathbf{Q}^+ = \hat{\mathbf{X}}\mathbf{diag}\left(\frac{1}{\mu_k}\right)\hat{\mathbf{X}}^T$, where the $N \times (N-1)$ matrix $\hat{\mathbf{X}}$ consists of all the normalized eigenvectors of $\mathbf{Q}$, except for the eigenvector $\mathbf{u}$ belonging to eigenvalue $\mu = 0$, and where the $(N-1) \times (N-1)$ diagonal matrix $\mathbf{diag}\left(\frac{1}{\mu_k}\right)$ contains the positive eigenvalues of Laplacian $\mathbf{Q}$.

The positive eigenvalues μ_k and the corresponding normalized eigenvector elements $\hat{\mathbf{X}}(v, k)$ of the weighted Laplacian of a path graph are [8]

$$\mu_k = 2b\left(1 - \cos\left(\frac{\pi k}{N}\right)\right),$$

$$\hat{\mathbf{X}}(v, k) = \frac{\sqrt{2}}{\sqrt{N}} \times \cos\left(\frac{\pi k v}{N} - \frac{\pi k}{2N}\right),$$

where $1 \le k \le N-1$, and $1 \le v \le N$. Then, the elements q_{ik}^+ of the pseudo-inverse of the Laplacian are

$$q_{ik}^+ = \sum_{v=1}^{N-1} \frac{\hat{\mathbf{X}}(i, v)\hat{\mathbf{X}}(k, v)}{\mu_v}. \tag{2.10}$$

Inserting the elements of pseudo-inverse in Eq. (2.10) and the power input $\mathbf{P} = [(N-1)p, 0, \ldots, 0, -(N-1)p]^T$ into the DC power flow equations in Eq. (2.9) results in the operating conditions, i.e., the phase angles Θ of node voltages, when the electric power is transferred from the supply node 1 to the demand node N:

$$\theta_i = p \times (N-1) \times (q_{i1}^+ - q_{iN}^+)$$
$$= \frac{p(N-1)(N-2i+1)}{2b}. \tag{2.11}$$

2.6.2 Operating Conditions in a Complete Graph

For a complete graph with equal link weights $b > 0$, the structure of the weighted Laplacian $\mathbf{Q}$ can be written as

$$\mathbf{Q} = b(N\mathbf{I} - \mathbf{J}), \tag{2.12}$$

where $\mathbf{J}$ is the all-one matrix, and $\mathbf{I}$ is the identity matrix. Using the definition of pseudo-inverse of the Laplacian [14]

$$\mathbf{Q}^+ = (\mathbf{Q} + \alpha\mathbf{J})^{-1}\left(\mathbf{I} - \frac{1}{N}\mathbf{J}\right), \tag{2.13}$$

where $\alpha > 0$ is a scalar, and choosing the scalar $\alpha = b$, the pseudo-inverse of the weighted Laplacian of a complete graph can be found as

$$\begin{aligned}\mathbf{Q}^+ &= (\mathbf{Q} + b\mathbf{J})^{-1}\left(\mathbf{I} - \frac{1}{N}\mathbf{J}\right) \\ &= \frac{1}{Nb}\left(\mathbf{I} - \frac{1}{N}J\right) = \frac{1}{N^2 b}(N\mathbf{I} - \mathbf{J}).\end{aligned} \tag{2.14}$$

From Eq. (2.9), the phase angles Θ of node voltages when the electric power transferred from the supply node 1 to the demand node N can be found as

$$\begin{aligned}\Theta &= \mathbf{Q}^+\mathbf{P} \\ &= \frac{1}{bN^2}\begin{bmatrix}(N-1) & -1 & \cdots & -1 \\ -1 & \ddots & & \vdots \\ \vdots & & \ddots & -1 \\ -1 & \cdots & -1 & (N-1)\end{bmatrix}\begin{bmatrix}(N-1)p \\ 0 \\ \vdots \\ -(N-1)p\end{bmatrix} = \frac{p}{bN}\begin{bmatrix}(N-1) \\ 0 \\ \vdots \\ -(N-1)\end{bmatrix}.\end{aligned}$$

2.6.3 Single Link Failure in a Path Graph

The failure and removal of a link l_{ik} from a network partitions its underlying graph if the equality between the reactance x_{ik} of the link and the effective resistance r_{ik} between its node pairs satisfies [10]

$$x_{ik} = r_{ik}.$$

When the underlying topology is a path graph, the effective resistance r_{ik} between nodes i and $k = i + 1$ can be written as

$$r_{ik} = |i - k| \times x_{ik},$$

meaning that the removal of any link l_{ik} partitions the path graph.

2.6.4 Single Link Failure in a Complete Graph

When a link l_{ik} with flow $|f_{ik}| = p$ is removed from the graph, the flow $|f_{ik}| = p$ through the link before its removal is redistributed over alternative paths between nodes i and k. Hence, the final flow through an arbitrary remaining link l_{ab} can be written as the sum of the previous state of the network, i.e., the previous flow through the link between nodes a and b when link l_{ik} is present, and the flow resulting from the change of the state due to the removal of link l_{ik}. The change in the flow Δf_{ab} through a remaining link l_{ab} can be calculated as [10]

$$\Delta f_{ab} = w_{ab} \times \frac{(r_{ak} - r_{ai} + r_{bi} - r_{bk})}{2(1 - w_{ik} \times r_{ik})} \times p, \tag{2.15}$$

where w_{ab} is the weight of the link l_{ab} and r_{ak} is the effective resistance between the nodes a and k.

The effective resistance between any two distinct nodes in the complete graph with equal link weights b is $\frac{2}{bN}$. Therefore, the numerator $(r_{ak} - r_{ai} + r_{bi} - r_{bk})$ of Eq. (2.15) is nonzero and its magnitude is equal to $|r_{ak} - r_{ai} + r_{bi} - r_{bk}| = \frac{2}{bN}$ only when the removed link l_{ik} and the observed link l_{ab} share a node. Then,

$$|\Delta f_{ab}| = \begin{cases} 0 & \text{if } l_{ik} \cap l_{ab} = \varnothing, \\ \frac{p}{N-2} & \text{otherwise.} \end{cases}$$

If the failure probabilities of the links in a complete graph are the same, we can calculate the probability p_r that a failed link is a *redundant* link with zero flow, and the probability p_u that a failed link is a *used* link with non-zero flow as

$$p_r = \frac{(N-1)(N-2)}{2} \times \frac{2}{N(N-1)} = \frac{N-2}{N} = 1 - \frac{2}{N}, \tag{2.16}$$

$$p_u = (N-1) \times \frac{2}{N(N-1)} = \frac{2}{N}, \tag{2.17}$$

where $p_u + p_r = 1$.

References

1. G.A. Pagani, M. Aiello, The power grid as a complex network: a survey. Phys. A: Stat. Mech. Appl. **392**(11), 2688–2700 (2013)
2. Y. Koç, M. Warnier, P. Van Mieghem, R.E. Kooij, F.M. Brazier, A topological investigation of phase transitions of cascading failures in power grids. Phys. A: Stat. Mech. Appl. **415**, 273–284 (2014)
3. M. Rosas-Casals, S. Valverde, R.V. Solé, Topological vulnerability of the European power grid under errors and attacks. Int. J. Bifurc. Chaos **17**(07), 2465–2475 (2007)

4. P. Crucitti, V. Latora, M. Marchiori, A topological analysis of the italian electric power grid. Phys. A: Stat. Mech. Appl. **338**(1), 92–97 (2004)
5. S. Trajanovski, J. Martín-Hernández, W. Winterbach, P. Van Mieghem, Robustness envelopes of networks. J. Complex Netw. **1**(1), 44–62 (2013)
6. E. Bompard, E. Pons, D. Wu, Extended topological metrics for the analysis of power grid vulnerability. IEEE Syst. J. **6**(3), 481–487 (2012)
7. X. Wang, E. Pournaras, R.E. Kooij, P. Van Mieghem, Improving robustness of complex networks via the effective graph resistance. Eur. Phys. J. B **87**(9), 221 (2014)
8. P. Van Mieghem, K. Devriendt, H. Cetinay, Pseudoinverse of the laplacian and best spreader node in a network. Phys. Rev. E **96**(3), 032311 (2017)
9. R.D. Zimmerman, C.E. Murillo-Sánchez, R.J. Thomas, Matpower: steady-state operations, planning, and analysis tools for power systems research and education. IEEE Trans. Power Syst. **26**(1), 12–19 (2011)
10. H. Cetinay, F.A. Kuipers, P. Van Mieghem, A topological investigation of power flow. IEEE Syst. J. (2016)
11. D. Van Hertem, J. Verboomen, K. Purchala, R. Belmans, W. Kling, Usefulness of DC power flow for active power flow analysis with flow controlling devices, in *Proceedings IET ACDC'06* (2006), pp. 58–62
12. Y. Koç, M. Warnier, R.E. Kooij, F.M. Brazier, An entropy-based metric to quantify the robustness of power grids against cascading failures. Saf. Sci. **59**, 126–134 (2013)
13. H. Cetinay, S. Soltan, F.A. Kuipers, G. Zussman, P. Van Mieghem, Comparing the effects of failures in power grids under the ac and dc power flow models. IEEE Trans. Netw. Sci. Eng. (2017)
14. P. Van Mieghem, *Graph Spectra for Complex Networks* (Cambridge University Press, Cambridge, 2010)